Thermochimica Acta 512 (2011) 233–239

Contents lists available at ScienceDirect

Thermochimica Acta

journal homepage: www.elsevier.com/locate/tca

Energy release characteristics of impact-initiated energetic aluminum–magnesium mechanical alloy particles with nanometer-scale structure

Yi Wang[a,b], Wei Jiang[a], Xianfeng Zhang[c], Hongying Liu[a], Yaqing Liu[b], Fengsheng Li[a,*]

[a] National Special Superfine Powder Engineering Research Center, Nanjing University of Science and Technology, Nanjing 210094, China
[b] School of Materials Science and Engineering, North University of China, Taiyuan 030051, China
[c] Department of Mechanical Engineering, Nanjing University of Science and Technology, Nanjing 210094, China

ARTICLE INFO

Article history:
Received 8 June 2010
Received in revised form
24 September 2010
Accepted 14 October 2010
Available online 5 November 2010

Keywords:
Mechanical alloying
Thermites
Nanostructure
Thermal reactivity
Impact-initiation

ABSTRACT

Aluminum–magnesium alloys, fabricated by bi-directional rotation ball milling, were used as a kind of promising solid fuel in "reactive material" that can be ignited by impact to release a large quantity of heats. Different percentages of Mg were added to Al to yield $Al_{90\%}$–$Mg_{10\%}$ and $Al_{70\%}$–$Mg_{30\%}$ alloys in order to probe the effect of Mg content on the microstructure and thermal reactivity of Al–Mg alloys. Structural characterization revealed that a nanometer-scale structure was formed and oxidation of as-fabricated alloy powders was faint. Moreover, as the Mg percentage increased, the particle size of alloy decreased with increasing brittleness of Al–Mg. TGA/DSC curves of the [$Al_{70\%}$–$Mg_{30\%}$]–O_2 system exhibited an intense exothermic peak before melting with reaction heat of 2478 J g^{-1} and its weight increase reached 90.16% of its theoretical value, which contrasted clearly with 181.2 J g^{-1} and 75.35% of [$Al_{90\%}$–$Mg_{10\%}$]–O_2 system, respectively. In addition, other than [$Al_{90\%}$–$Mg_{10\%}$]–Fe_2O_3 system, the [$Al_{70\%}$–$Mg_{30\%}$]–Fe_2O_3 system exhibited a considerable solid–solid reaction and a low activation energy. Finally, target penetration experiments were conducted and the results confirmed that a projectile composed of [$Al_{70\%}$–$Mg_{30\%}$]–Fe_2O_3 displayed a more complete ignition of target than that of Al–Fe_2O_3 formulation.

1. Introduction

The term "reactive materials" denotes a class of energetic materials that generally combines two or more non-explosive solids. The compositions have features of high density, high energy release, low sensitivity (such as impact, friction, shock, electric spark, and flame sensitivities), and can be initiated by a strong impact to release a large quantity of chemical energy [1–4]. There is interest in enhancing the power of warheads and projectiles by including "reactive materials" in them, such as making reactive fragments and replacing standard metal liners in shaped charges or using explosively formed penetrators [5–7]. A number of studies have indicated that many types of metastable materials may be used as "reactive materials"; thermites are promising because of their large exothermicity, high density, reliable safety, and thermal properties that can be readily tailored by varying the oxidizer to fuel ratio [8–12]. Ferranti found that the reactive velocity of an Al–Fe_2O_3–epoxy resin reactive fragment reached 163 m s^{-1} after impact initiation [2]. Baker investigated the penetration performance of powder liners composed of "reactive materials" with fuel-rich, oxygen-rich, and neutral fuel–oxygen balance, and their results indicated that the active liner destroyed a concrete structure more effectively than the common Al liner [7]. Notably, Dolgoborodov prepared an Al/Teflon composite by mechanical ball milling and mold-pressing to give a highly compact and high-hardness pellet [1]. The experiments revealed that the Al/Teflon pellet impact-initiated and generated a deflagration, with a maximum deflagration velocity of 1.28 km s^{-1}.

The research described above confirmed the feasibility of using thermites as "reactive materials" but also exposed the deficiency of traditional thermites. Because they are composites, the reaction mechanism of thermites is different due to their granular nature from that of monomolecular energetic materials. Traditional thermites are generally composed of coarse Al particles present poor reactivity characteristics such as a low burning rate, poor heat release, and high ignition temperatures (T_{ign} > 900 °C) and because of which they are not suitable for use as "reactive materials" and found no further application [13]. Much research has been conducted to solve this problem, investigating options such as the implementation of mechanical milling or the use of

* Corresponding author. Tel.: +86 025 84315942.
E-mail addresses: wangyi528528@yahoo.com.cn, wangyi528528@163.com (F. Li).

0040-6031/$ – see front matter © 2010 Elsevier B.V. All rights reserved.
doi:10.1016/j.tca.2010.10.013

Al nanoparticles as fuel. Umbrajkar prepared an Al/CuO nanocomposite with coarse Al (40 μm) and CuO (1–5 μm) powders by arrested reactive milling [14]. He found that ignition of the Al/CuO nanocomposites was driven primarily by the lower-temperature oxidation processes. Plantier blended Al nanoparticles with Fe(III) oxide nanoparticles and found that the maximal burn rate of this nano-sized thermite reached 617 m s^{-1} [11]. Valliappan's experiments also indicated that the average combustion front velocity of the nanometer Al–WO_3 system was 412 m s^{-1}, i.e., more than a 50-fold increase over the coarse Al–WO_3 system [15].

Therefore, it is possible that enhancing the thermal reactivity of Al particles may potentially improve the performance of thermites. In our previous report, coating micron-sized Al with nanometer-sized metal particles by a displacement method overcame the poor reaction mechanism, i.e., the active Al particles encased in unreactive Al_2O_3 layers [16,17]. However, it is difficult to mass-produce the Al/metal nanocomposites due to the erosive reaction between Al and water. Alternatively, powders of metastable Al-based alloys have been proposed as promising solid fuels with high reactivity and high energy release to improve the performance of propellants and thermites. Shoshin fabricated metastable Al–Ti mechanical alloys of $Al_{0.90}Ti_{0.10}$, $Al_{0.85}Ti_{0.15}$, $Al_{0.80}Ti_{0.20}$, and $Al_{0.75}Ti_{0.25}$ and studied their ignition and combustion [18,19]. He found that the oxidation of Al–Ti alloys was no longer restricted by surface Al_2O_3 layers, and $Al_{0.75}Ti_{0.25}$ was ignited at 830 K and observed blazing burning at 900 K, at a heating rate of 3000 K s^{-1}. These results are impossible using coarse Al powder.

Because Ti is expensive, a good alternative is Mg for promoting the reactivity of coarse Al. Shoshin prepared Al–Mg solid solutions by mechanical alloying [20]. The experimental results indicated that the grain size sharply decreased from more than 100 nm (pure Al) to 6 nm ($Al_{0.50}Mg_{0.50}$) after alloying. In addition to the decrease in grain size, the ignition temperatures of $Al_{0.90}Mg_{0.10}$ and $Al_{0.80}Mg_{0.20}$ fell to 1170 K and 1095 K, respectively, compared with about 2300 K for pure Al. When the Mg content increased to 50 wt.%, the ignition temperature of the alloy shifted to that of pure Mg powder (about 980 K). Moreover, the Al–Mg alloy exhibited a higher burning rate and flame temperature than pure Al powder in air.

To a large degree, the thermal reactivity of coarse Al was improved by the mechanical alloying of Al with another metal. Good ignition determines whether the solid fuel can be applied as a reactive material. For Al–Mg alloys, the loose MgO layer and the nanostructure formed from mechanical alloying are two important factors for free oxidation and good ignition. Moreover, the oxidation of Mg, accompanied with a mass heat release, will less depress the energy of the solid fuel. However, excess Mg will decrease the sensitivity of the "reactive materials". For example, in the course of pelleting, the exothermic reaction between available Al–Mg and H_2O will lead to inactivation of the fuel.

Therefore, although alloying with Mg can improve the oxidation of Al powder, the content of Mg must optimized to keep a balance between reactivity and sensitivity. Bi-directional rotation ball milling was employed in this research to fabricate Al–Mg mechanical alloy particles with nanometer-scale structure, and their energy release characteristics were investigated in detail.

2. Experimental

2.1. Materials

Raw Al powder (99.9% purity) was purchased from Hongwu Nanometer Materials Ltd., China. Coarse Mg particles (99% purity, 80–200 mesh) were obtained from Sinopharm Chemical Reagent Co., Ltd., China. The Al and Mg powders were used as starting materials. Stearic acid (C.P.) as a grinding agent, *n*-hexane (A.R.), and Fe_2O_3 powders were purchased from Shanghai Chemical Ltd., China.

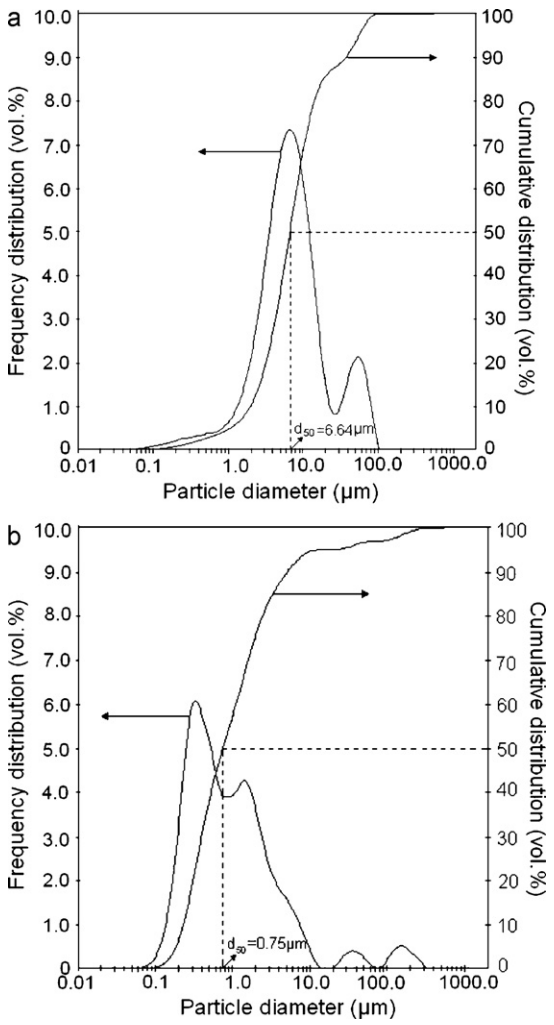

Fig. 1. Particle size distribution diagrams of $Al_{90\%}$–$Mg_{10\%}$ (a) and $Al_{70\%}$–$Mg_{30\%}$ (b): d_{50} is the median diameter of the sample.

2.2. Fabrication

A 1000-g mixture of Al and Mg (10 or 30 wt.% magnesium) was introduced into a ball mill and the machine was started without any milling balls. After 30 min, stainless steel balls with diameters of 2–8 mm were added into the mill and cooling water was circulated. After running a period of time in which stearic acid (1.5–5 wt.% of the materials) was added at a certain break, the machine was stopped and an N_2/O_2 (2–5 vol.% O_2) gas was passed through the cavity in another 48 h. After this process, the $Al_{90\%}$–$Mg_{10\%}$ or $Al_{70\%}$–$Mg_{30\%}$ alloy had been fabricated.

According to the specific mass-proportion of Al to Mg within each alloy, the thermites were prepared by mixing the fuel and oxidizer stoichiometrically according to Eqs. (1) and (2) [21]

$$\mathrm{Al} + \frac{1}{2}\mathrm{Fe_2O_3} \rightarrow \mathrm{Fe} + \frac{1}{2}\mathrm{Al_2O_3} + 4.003 \quad \mathrm{kJ\ g^{-1}_{Thermite}} \tag{1}$$

$$\mathrm{Mg} + \frac{1}{3}\mathrm{Fe_2O_3} \rightarrow \frac{2}{3}\mathrm{Fe} + \mathrm{MgO} + 1.775 \quad \mathrm{kJ\ g^{-1}_{Thermite}} \tag{2}$$

The mixtures of the fuel ($Al_{90\%}$–$Mg_{10\%}$, $Al_{70\%}$–$Mg_{30\%}$, or pure Al) and oxidizer (Fe_2O_3) were ultrasonicated in *n*-hexane, heated at low temperature in vacuum to evaporate the *n*-hexane, and finally sifted through a wire mesh of 200 μm to obtain the thermites used

in this investigation. To contrast the impact-initiated characteristics of pure Al and Al–Mg alloys, two kinds of thermites blends with a moderate gas-forming agent, seldom catalyst, and a minimum of binder were pressed to highly compact, high-hardness pellets (ϕ 10 mm × 10 mm).

2.3. Characterization

The morphology and surface elements of the samples were examined by an S-4800 field-emission scanning electron microscope (SEM) coupled with energy dispersive spectroscopy (EDS). Differential scanning calorimetry of the thermites was performed on a TA Model Q600 differential scanning calorimeter from room temperature to 1100 °C in air or argon gas flowing at 10 mL min^{-1}, and heating rates of 5, 10, and 20 K min^{-1} were adopted. The phase variations of Al–Mg alloys were investigated by a Bruker Advance D8 X-ray diffractometer, using Cu Kα radiation at 40 kV and 30 mA. The selected still-frame photographs for the impact testing of the thermite pellets were recorded by a high speed camera (Vision Research).

3. Results and discussion

3.1. Structural characterization

The particles size distributions of the fabricated powders were measured and the diagrams were presented in Fig. 1. By means of cumulative distribution curve, the median diameter (d_{50}) of $Al_{90\%}$–$Mg_{10\%}$ and $Al_{70\%}$–$Mg_{30\%}$ were calculated as the results of 6.64 μm and 0.75 μm, respectively. Diminution of particle size implies decreasing the ductility of the Al–Mg powder as the Mg content increases from 10 wt.% to 30 wt.%. In virtue of frequency distribution curve, the broad size distribution was inferred for both samples, and the multi-peaks mean the heterogeneous particle size distribution because it is impossible to control whole powder material subjected to a same mechanical actions in the course of milling.

The representative electron microscope images of the Al–Mg alloys particles are shown in Fig. 2. Fig. 2(a–c) indicates that microscopic morphology of the alloy particles are as granular as well-dispersible and plump granules instead of agglomerative flake. Accordingly, alloying with Mg increases the brittleness of the Al powder that should have been ground into flakes after milling due to the intrinsic ductility. The granular structure expands the effective application of this solid fuel because it helps ensure a high charge density. At a magnification of 150,000×, it is quite clear that the surface of $Al_{90\%}$–$Mg_{10\%}$ and $Al_{70\%}$–$Mg_{30\%}$ particles are both structured on nanometer scale with a high surface roughness. EDS spectra (Fig. 3) indicate that the surface of the $Al_{90\%}$–$Mg_{10\%}$ particles primarily contains aluminum, implying that the Mg element went into solid solution with the Al due to the milling. In addition, the appearance of a faint O peak indicates minor oxidation of the $Al_{70\%}$–$Mg_{30\%}$.

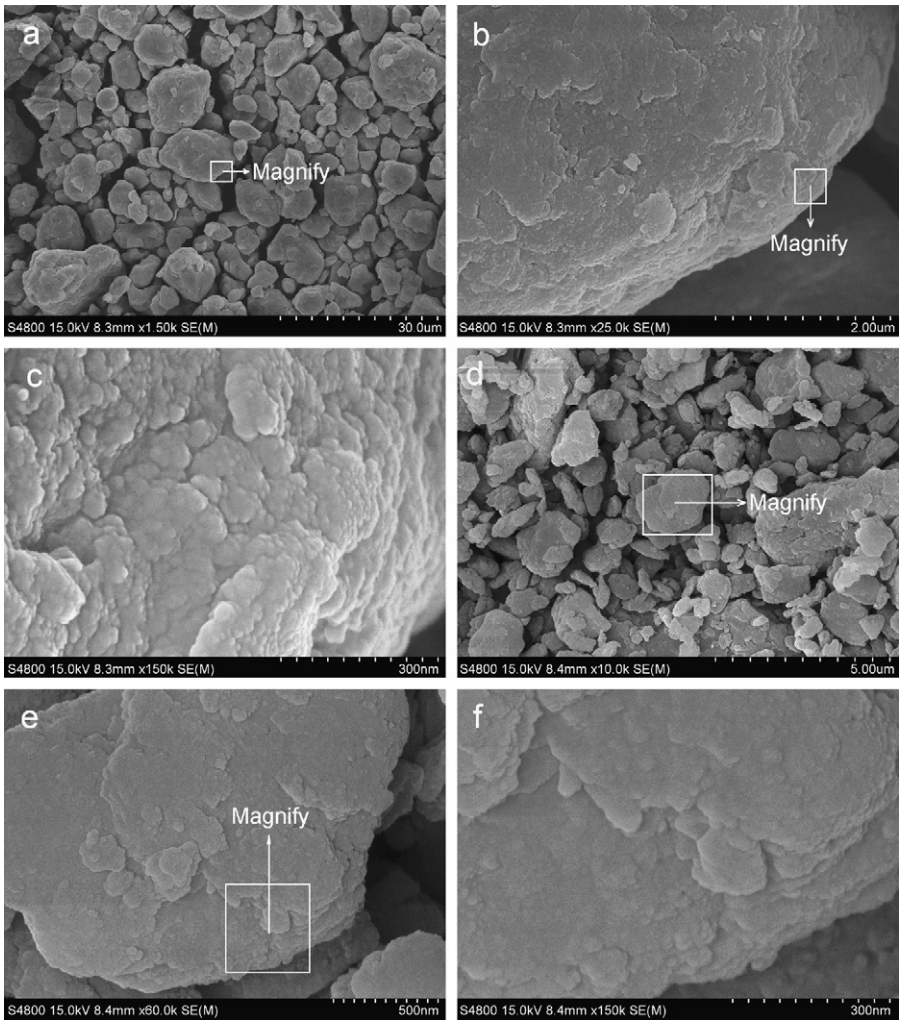

Fig. 2. SEM images of $Al_{90\%}$–$Mg_{10\%}$ (a–c) and $Al_{70\%}$–$Mg_{30\%}$ (d–f): (b), (c), (e), and (f) are the enclosed surface shown in (a), (b), (d), and (e), respectively.

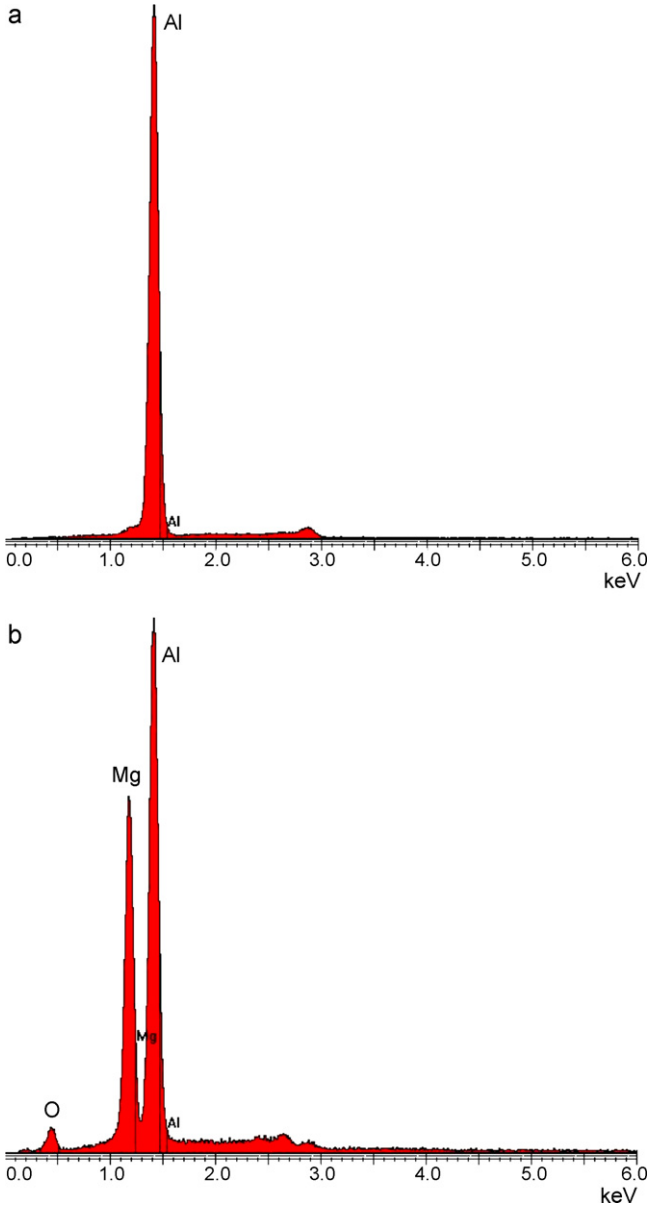

Fig. 3. EDS spectra of $Al_{90\%}$–$Mg_{10\%}$ (a) and $Al_{70\%}$–$Mg_{30\%}$ (b).

Fig. 4 displays the X-ray diffraction patterns of two Al–Mg alloys. It is obvious that the Al–Mg solid solution phase was produced by mechanical alloying, although faint peaks for intermetallic Al_3Mg_2 and Mg exist. MID jade5.0 software was employed for peak fitting, and the average crystallite size of 21.7 nm for $Al_{90\%}$–$Mg_{10\%}$ and 25.4 nm for $Al_{70\%}$–$Mg_{30\%}$ were calculated with the peaks located at a 2θ of 38°.

3.2. Thermal analysis

3.2.1. Oxidation in air

Fig. 5 illustrates the TGA/DSC traces of $Al_{90\%}$–$Mg_{10\%}$ and $Al_{70\%}$–$Mg_{30\%}$. In each DSC curve, the endothermic peak at about 660 °C, i.e., the theoretical melting point of aluminum, is observed and may be associated with the melting of Al–Mg alloys. Before and after the melting point, two exothermic peaks indicate two courses of oxidation for the alloys. The peak at about 620 °C for $Al_{70\%}$–$Mg_{30\%}$ is highly exothermic and its oxidation heat of 2478 J g^{-1} is about a 14-fold increase compared with

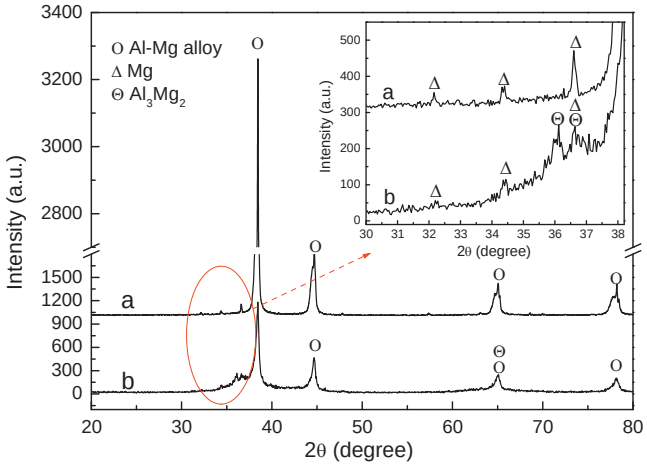

Fig. 4. XRD patterns of $Al_{90\%}$–$Mg_{10\%}$ (a) and $Al_{70\%}$–$Mg_{30\%}$ (b): the inset graph is a magnification of the area in the circle.

$Al_{90\%}$–$Mg_{10\%}$. Furthermore, for $Al_{70\%}$–$Mg_{30\%}$, the intensity and heat of its solid–gas reaction are distinctly higher than those of its liquid–gas reaction occurring at about 990.5 °C, which is attributed to its nanostructured surface and the very fine alloy particles. In addition, the high temperature reaction of $Al_{70\%}$–$Mg_{30\%}$ has precedence over the incomplete exothermic peak of $Al_{90\%}$–$Mg_{10\%}$. TGA data indicate that the oxidation of $Al_{70\%}$–$Mg_{30\%}$ is more complete because its weight increase ratio (the ratio of the actual

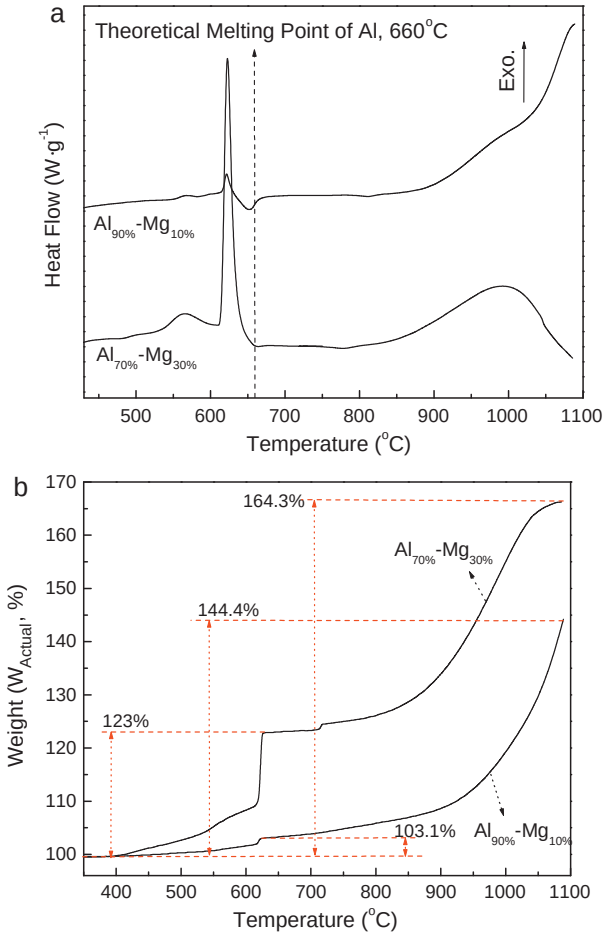

Fig. 5. TGA/DSC traces of the alloys at a heating rate of 20 K min^{-1} in the air.

Table 1
Thermal analysis data of Al–Mg alloy heated in air.

Alloy	ΔH_r (low) (J g^{-1})	ΔH_r (high) (J g^{-1})	W_{Actual} (%)	$\frac{W_{Actual}}{W_{Theoretical}} \times 100\%$ (%)
$Al_{90\%}$–$Mg_{10\%}$	181.2	–	144.39	75.35
$Al_{70\%}$–$Mg_{30\%}$	2478	2169	164.31	90.16

weight increase to the theoretical weight increase) is higher (see Table 1).

3.2.2. Thermite reaction

As thermite fuels, reactions of Al–Mg alloys with Fe_2O_3 were investigated by thermal analysis. Results in Fig. 6 manifest the considerable differences in reactivity between $Al_{70\%}$–$Mg_{30\%}$ and $Al_{90\%}$–$Mg_{10\%}$. Unlike [$Al_{90\%}$–$Mg_{10\%}$]–Fe_2O_3, the [$Al_{70\%}$–$Mg_{30\%}$]–Fe_2O_3 system released more heat at 545.3–584.1 °C, and its high temperature reaction occurred at a lower temperature, which implies a distinct solid–solid reaction as well as good ignition.

The representative DSC data of thermite reactions for two [Al–Mg]–Fe_2O_3 systems at heating rate of 20 K min^{-1} in high pure Ar were listed in Table 2. It is found that the diminished theoretical value of reaction heat is responsible to increasing mass ratio of Mg to Al. However, the actual heat released, as compensating for decrease of theoretical energy, enhances significantly if the percent of added Mg increased to 30%. Remarkably, the solid–solid reaction of [$Al_{70\%}$–$Mg_{30\%}$]–Fe_2O_3 system is more considerable accounting for the 309.4 J g^{-1} higher of reaction heat than the counterpart of [$Al_{90\%}$–$Mg_{10\%}$]–Fe_2O_3 system. Meanwhile, under the same condition, the values of Q_{max} (the maximum heat-flow at individual peak point) were employed to simply assess the intensity of thermite reaction. Comparing the data in Table 2, it is no doubt that in the same duration, [$Al_{70\%}$–$Mg_{30\%}$]–Fe_2O_3 may release more heat than [$Al_{90\%}$–$Mg_{10\%}$]–Fe_2O_3 system.

The Starink method was used in the kinetic evaluation of the thermite DSC traces obtained at different heating rates [22–25]

$$\ln\left(\frac{T_p^{1.8}}{\varphi}\right) = A \cdot \frac{E_a}{RT_p} + C \quad (3)$$

where T_p is a peak temperature in the DSC curve in Kelvin; φ is the heating rate in K min^{-1}; E_a is the activation energy in J mol^{-1}; A is pre-exponential factor, as is an expression of $1.0070 - 1.2 \times 10^{-8} E_a$; R is gas constant of 8.314 J mol^{-1} K^{-1}; C is a constant. Meanwhile because the values of R^2 in Table 3 (symbol R^2 is used to identify the linear coefficient of $\ln(T_p^{1.8} \cdot \varphi^{-1})$ to $10^4 \cdot T_p^{-1}$) display some difference between samples, the final acti-

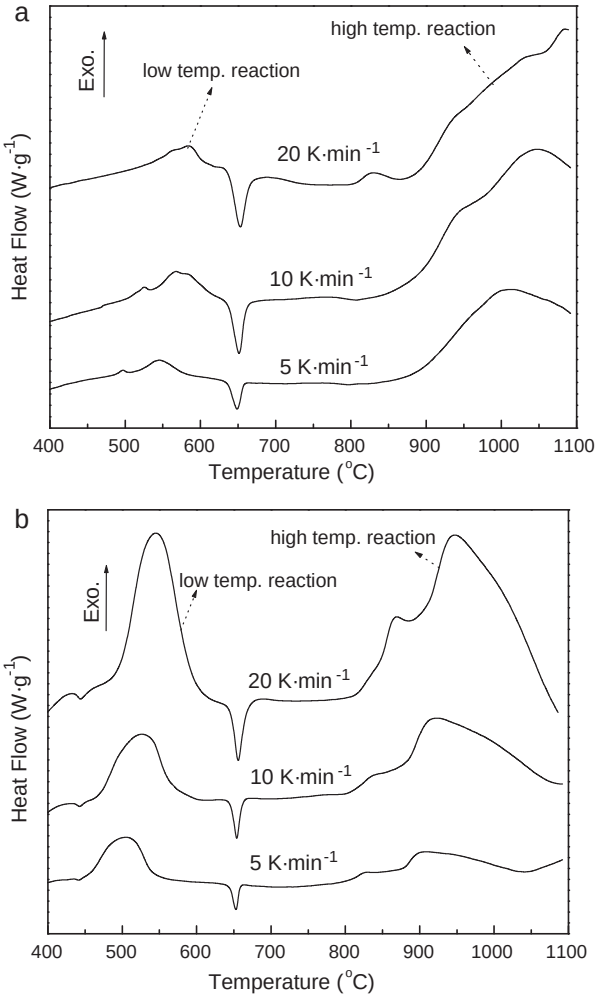

Fig. 6. DSC traces of alloys obtained at different heating rates: (a) [$Al_{90\%}$–$Mg_{10\%}$]–Fe_2O_3 and (b) [$Al_{70\%}$–$Mg_{30\%}$]–Fe_2O_3.

Table 2
Thermodynamic parameters of the thermite reaction for [Al–Mg]–Fe_2O_3 systems.

Thermites	ΔH_r (low) (J g^{-1})	ΔH_r (high) (J g^{-1})	ΔH_r (theoretical) (J g^{-1})	Q_{max} (low) (W g^{-1})	Q_{max} (high) (W g^{-1})
[$Al_{90\%}$–$Mg_{10\%}$]–Fe_2O_3	74.3	–	3780.2	0.40	1.53
[$Al_{70\%}$–$Mg_{30\%}$]–Fe_2O_3	383.7	697.6	3334.6	1.65	1.64

Table 3
Kinetics parameters of the thermite reaction for [Al–Mg]–Fe_2O_3 systems.

Reaction types	Thermites	ϕ (K min^{-1})	$\ln(T_p^{1.8} \cdot \varphi^{-1})$	$10^4 \cdot T_p^{-1}$ (K^{-1})	R^2	$\bar{E}_a$ (kJ mol^{-1})
Solid–solid reaction (low temperature)	[$Al_{90\%}$–$Mg_{10\%}$]–Fe_2O_3	5	10.446	12.206	0.990	203.762
		10	9.820	11.891		
		20	9.161	11.666		
	[$Al_{70\%}$–$Mg_{30\%}$]–Fe_2O_3	5	10.371	12.863	0.995	167.355
		10	9.729	12.503		
		20	9.078	12.218		
Liquid–solid reaction (high temperature)	[$Al_{90\%}$–$Mg_{10\%}$]–Fe_2O_3	5	11.275	7.788	0.998	247.159
		10	10.629	7.583		
		20	9.991	7.357		
	[$Al_{70\%}$–$Mg_{30\%}$]–Fe_2O_3	5	11.108	8.545	0.999	312.416
		10	10.451	8.372		
		20	9.796	8.197		

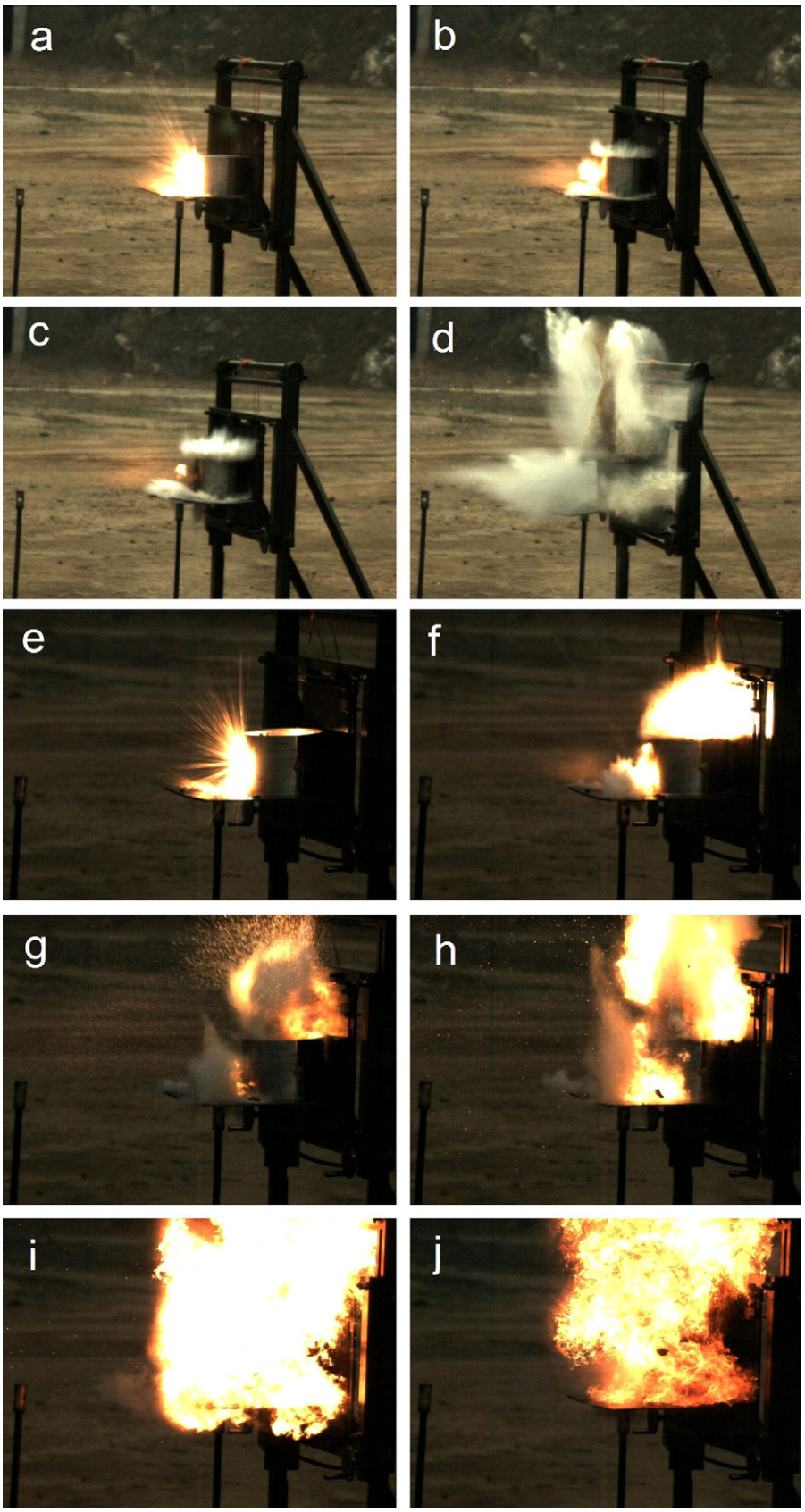

Fig. 7. Frames from high-speed video of the impact and reaction process for thermite pellets composed of Al–Fe_2O_3 (a–d) and [$Al_{70\%}$–$Mg_{30\%}$]–Fe_2O_3 (e–j).

vation energy of each sample is expressed as an average value of E_a ($\overline{E}_a$) calculated from Starink's formula with DSC data collected at every two heating rates.

$$\overline{E}_a = \frac{1}{3} \cdot \sum_{i,j} E_{a(i-j\ \mathrm{K\ min^{-1}})} \quad (4)$$

where array (i,j) of heating rate refers to (5, 10), (5, 20), or (10, 20), respectively, and $E_{a(5-10\ \mathrm{K\ min^{-1}})}$, $E_{a(5-20\ \mathrm{K\ min^{-1}})}$ and $E_{a(10-20\ \mathrm{K\ min^{-1}})}$ are the activation energies calculated from Eq. (3) by Starink's method.

Results listed in Table 3 indicate that the increasing Mg content decreases the activation energy of the solid–solid reaction between the Al–Mg alloy and ferric oxide. However, for the high temperature reaction, the $\overline{E}_a$ of [$Al_{70\%}$–$Mg_{30\%}$]–Fe_2O_3 increased by 65.257 kJ mol^{-1}, which can be ascribed to the obstruction of residue generated from the solid–solid reaction.

3.3. Impact-initiation characteristics

In our study, the goal of mechanical alloying Al with Mg is to obtain a kind of real reactive material that can release a large quantity of energy when it undergoes a severe impact action, for which the impact-initiated energy release characteristics were tested by target penetration experiments. The target was a sealed steel jar (roughly ϕ 40 cm × 40 cm) filled with diesel oil. The pressed thermite pellet was used as a bullet core and was inserted into a projectile, which was shot by a gun. Due to its low volatility and high knocking critical point, the diesel oil cannot be ignited until the thermite pellet releases enough energy, resulting in a very high flame temperature.

The selected still-frame photographs of the impact and reaction processes from high-speed video are shown in Fig. 7. Fig. 7(a–d) exhibits the impact event of an Al–Fe_2O_3 thermite pellet. It is very clear that although the impact action ignited the column, the flame was soon extinguished by the diesel–oil because this chemical reaction released insufficient energy and generated a weak deflagration. In contrast, the projectile charged with [$Al_{70\%}$–$Mg_{30\%}$]–Fe_2O_3 destroyed the target in complete ignition, instead of the incomplete ignition by that charged with Al–Fe_2O_3 thermite.

4. Conclusion

As solid fuels with high thermal reactivities, Al–Mg alloys with different Mg contents were fabricated using mechanical ball milling with bi-directional rotation. Structural characterization indicated that introducing Mg increased the brittleness of Al and the average crystallite size of Al–Mg alloys decreased to 21.7–25.4 nm after extended ball milling.

Thermal analysis results indicated that $Al_{70\%}$–$Mg_{30\%}$ was intensively oxidized in the solid state, while $Al_{90\%}$–$Mg_{10\%}$ was not. The weight increase of $Al_{90\%}$–$Mg_{10\%}$ and $Al_{70\%}$–$Mg_{30\%}$ in air, about 75.35% and 90.16% of their respective theoretical values, indicated effective oxidation. Moreover, an obvious solid–solid state reaction also appeared in the DSC traces of the [$Al_{70\%}$–$Mg_{30\%}$]–Fe_2O_3 system in a pure Ar atmosphere. For the same thermite, its solid–solid reaction activation energy was lower than that of the liquid–solid reaction. These results strongly suggest that mechanical alloying with Mg is a good approach to substantially improving the ignition and reactivity of coarse Al particles.

Target penetration experiments, conducted using thermite pellets as projectiles and sealed steel jars filled with diesel oil as targets confirmed that the projectile composed of [$Al_{70\%}$–$Mg_{30\%}$]–Fe_2O_3 displayed a suitable impact-initiated characteristics for use as a kind of impact-initiated reactive material, given its effective destruction of the target with good ignition.

Acknowledgments

This work was supported by a National Nature & Science Fund of China (Grant: 50972060). The authors would like to thank the Hongyang Machinery Factory for their enthusiastic support of our experiments.

References

[1] A.Y. Dolgoborodov, M.N. Makhov, I.V. Kolbanev, JETP Lett. 81 (7) (2006) 311–314.
[2] L. Ferranti, N.N. Thadhani, Mater. Res. Soc. (2006) 588–610.
[3] E.M. Hunt, S. Malcolm, M.L. Pantoya, Int. J. Impact Eng. 36 (2009) 842–846.
[4] A.Y. Dolgoborodov, A.N. Streletskii, M.N. Makhov, Russ. J. Phys. Chem. B, Focus Phys. 1 (6) (2008) 606–611.
[5] D. Spitzer, M. Comet, C. Baras, J. Phys. Chem. Solids 71 (2010) 100–108.
[6] Comm. Adv. Energetic Mater. Manufacturing Technol., Advanced Energetic Materials, National Academies Press, Washington, 2004.
[7] E.L. Baker, A.S. Daniels, K.W. Ng, in: 19th International Symposium on Ballistics, 2001, pp. 569–574.
[8] M.L. Pantoya, J.J. Granier, J. Therm. Anal. Calorim. 85 (1) (2006) 37–43.
[9] D. Stamatis, Z. Jiang, V.K. Hoffmann, Combust. Sci. Technol. 181 (2009) 97–116.
[10] J. Sun, M.L. Pantoya, S.L. Simon, Thermochim. Acta 444 (2006) 117–127.
[11] K.B. Plantier, M.L. Pantoya, A.E. Gash, Combust. Flame 140 (2005) 299–309.
[12] K. Sullivan, G. Young, M.R. Zachariah, Combust. Flame 156 (2009) 302–309.
[13] S.X. Wang, K.M. Liang, X.H. Zhang, J. Mater. Sci. Lett. 22 (2003) 855–856.
[14] S.M. Umbrajkar, M. Schoenitz, E.L. Dreizin, Thermochim. Acta 451 (2006) 34–43.
[15] S. Valliappan, J. Swiatkiewicz, J.A. Puszynski, Powder Technol. 156 (2005) 164–169.
[16] Y. Wang, W. Jiang, Z.P. Cheng, Thermochim. Acta 463 (2007) 69–76.
[17] Y. Wang, W. Jiang, Z.P. Cheng, Rare Metal Mater. Eng. 37 (7) (2008) 1197–1200.
[18] Y.L. Shoshin, M.A. Trunov, X.Y. Zhu, Combust. Flame 144 (2006) 688–697.
[19] Y.L. Shoshin, E.L. Dreizin, Combust. Flame 145 (2006) 714–722.
[20] Y.L. Shoshin, R.S. Mudryy, E.L. Dreizin, Combust. Flame 128 (2002) 259–269.
[21] R.H. Perry, D.W. Green, Perry's Chemical Engineers Handbook, vol. 2, Sci. Press, Beijing, 2001.
[22] M.J. Starink, Thermochim. Acta 288 (1996) 97–104.
[23] M.J. Starink, Thermochim. Acta 404 (2003) 163–176.
[24] S. Vyazovkin, C.A. Wight, Annu. Rev. Phys. Chem. 48 (1997) 125–149.
[25] X.L. Song, Y. Wang, C.W. An, J. Hazard. Mater. 159 (2008) 222–229.